WAVEFORM-AGILE SENSING FOR TRACKING MULTIPLE TARGETS IN CLUTTER

Sandeep P. Sira[†]*, Antonia Papandreou-Suppappola*[†]*, Darryl Morrell*[‡]*, Douglas Cochran*[§]

[†]Department of Electrical Engineering, [‡]Department of Engineering,
[§]Ira A Fulton School of Engineering,
Arizona State University

ABSTRACT

In this paper, we consider the problem of scheduling the waveform transmitted by waveform-agile radar sensors to track multiple targets in clutter. A number of generalized frequency modulated chirps with trapezoidal envelope form the library of waveforms available to the sensors, which obtain measurements using a nonlinear observation model. A joint probabilistic data association filter is used to track the target, and the waveform selection is made so as to minimize the predicted mean square tracking error. We provide simulation results to show that the scheduling improves the tracking performance of multiple targets even in the presence of clutter.

1. INTRODUCTION

As sensors become increasingly capable and intelligent, it has become possible to consider their dynamic adaptation in response to changes in their environment and task. In radar systems, for example, the ability to change the transmitted waveform on a pulse-by-pulse basis can obtain important information about targets that contributes optimally to achieving the system's objective. In target tracking applications, the objective could be the maximization of detection probability, minimization of tracking error, or choice of sensor usage. Waveform adaptation methods that integrate the sensor and the tracker result in a system-level optimization that can deliver better performance than when each component is optimized independently.

Waveform adaptive algorithms can typically determine a schedule of waveforms to be transmitted over a specified time horizon so as to minimize (or maximize) a suitably chosen performance criterion. The dynamic selection of waveforms for target tracking was first considered in [1], where the optimal waveform parameters were derived for tracking one-dimensional target motion using a linear observations model with perfect detection in a clutter-free environment. Here, the solution to the myopic or one-step-ahead waveform selection problem was obtained in closed form since both performance metrics (tracking error and validation gate volume) could be computed in closed form. This is usually not possible when nonlinear observations models are used, as is often the case in modern tracking scenarios. A combined optimization of the detection threshold and the transmitted waveform for target tracking was presented in [2], where a cost function based on the cumulative probability of track loss and the target state covariance was minimized. Recently, the development of waveform libraries for target tracking was studied in [3] where an information theoretic criterion was maximized. The waveform scheduling problem for tracking a single target in clutter was considered in [4].

In scenarios that include clutter and multiple targets, the tracking algorithm must estimate the association between the measurements and the targets. Waveform adaptation in this scenario becomes challenging since the effect of the uncertainty in the origin of the measurements must be incorporated in the mechanism to predict the cost of using a particular waveform. While the work in [1] was extended to include clutter in [5], waveform selection for tracking multiple targets was not considered.

In this paper, we present an algorithm that configures two radar sensors to track multiple targets using waveforms with different time-frequency signatures so as to dynamically exploit their resolution in estimating delay and Doppler. Specifically, the frequency modulation (FM), duration and FM rate for linear and nonlinear chirps are chosen so as to minimize the predicted mean square error (MSE). The MSE is predicted using the Cramèr-Rao lower bound (CRLB) on the measurement error variance. The observations are used by a joint probabilistic data association filter to track targets that move in two dimensions. By means of a numerical simulation example, we compare the tracking error resulting from using sensors in fixed and dynamic configurations and demonstrate the improvement afforded by our configuration algorithm. The reduced estimation errors would be useful for both tracking over a time period as well as localizing multiple targets at a specific time step.

This work was partly supported by the Department of Defense, administered by the Air Force Office of Scientific Research Grant No. AFOSR FA9550-05-1-0443, and by the DARPA WAS program under NRL grant N00173-06-1-G006.

The paper is organized as follows. In Section 2, we describe the target dynamics and the measurement and clutter models. Section 3 describes the waveform structure and develops the measurement noise covariance matrix. The target tracking algorithm using a particle filter with probabilistic data association is presented in Section 4 while in Section 5, we propose the waveform configuration algorithm. Section 6 presents a simulation study.

2. STATE-SPACE AND CLUTTER MODELS

2.1. Target dynamics

Let $\mathbf{X}_k = [\mathbf{x}_k^{1^T}, \ldots, \mathbf{x}_k^{S^T}]^T$ represent the state of S targets that move in a two-dimensional space. The state of target s, $s = 1, \ldots, S$ is $\mathbf{x}_k^s = [x_k^s \ y_k^s \ \dot{x}_k^s \ \dot{y}_k^s]^T$, where x_k^s and y_k^s correspond to the position, and $\dot{x}_k^s$ and $\dot{y}_k^s$ to the velocity at time k in Cartesian coordinates. The dynamics of each target are modeled by a linear, constant velocity model given by

$$\mathbf{x}_k^s = F\,\mathbf{x}_{k-1}^s + \mathbf{w}_k^s, \tag{1}$$

where $\mathbf{w}_k^s$ is a white Gaussian noise sequence that models the process noise. The constant matrix F and the process noise covariance matrix Q are

$$F = \begin{bmatrix} 1 & 0 & \delta t & 0 \\ 0 & 1 & 0 & \delta t \\ 0 & 0 & 1 & 0 \\ 0 & 0 & 0 & 1 \end{bmatrix}$$

$$Q = q \begin{bmatrix} \frac{\delta t^3}{3} & 0 & \frac{\delta t^2}{2} & 0 \\ 0 & \frac{\delta t^3}{3} & 0 & \frac{\delta t^2}{2} \\ \frac{\delta t^2}{2} & 0 & \delta t & 0 \\ 0 & \frac{\delta t^2}{2} & 0 & \delta t \end{bmatrix} \tag{2}$$

where δt is the sampling interval and q is a constant.

2.2. Measurement model

At each sampling epoch, each of two waveform-agile, active sensors, Sensor A and Sensor B, obtain range (r) and range-rate ($\dot{r}$) measurements of each target. At time k, the measurement corresponding to target s obtained at sensor i, $i =$ A, B, is given by

$$\mathbf{z}_k^{s,i} = h^i(\mathbf{x}_k^s) + \mathbf{v}_k^{s,i} \tag{3}$$

where $\mathbf{v}_k^{s,i}$ is a white Gaussian noise sequence that models the measurement error. We assume that $\mathbf{v}_k^{s,i}$ in (3) is independent between all targets and sensors, and that $\mathbf{v}_k^{s,i}$ and $\mathbf{w}_k^s$ in (1) are uncorrelated for all targets. The nonlinear function $h^i(\mathbf{x}_k^s) = [r_k^{s,i} \ \dot{r}_k^{s,i}]^T$, where

$$r_k^{s,i} = \sqrt{(x_k^s - x^i)^2 + (y_k^s - y^i)^2}$$
$$\dot{r}_k^{s,i} = (\dot{x}_k^s(x_k^s - x^i) + \dot{y}_k^s(y_k^s - y^i))/r_k^{s,i}$$

and sensor i is located at (x^i, y^i).

2.3. Clutter model

The measurement at time k consists of false alarms due to clutter as well as the target returns for each detected target. For sensor i, the measurement is given by

$$\mathbf{Z}_k^i = [\mathbf{z}_{k,1}^i \ \mathbf{z}_{k,2}^i \ \ldots \mathbf{z}_{k,m_k^i}^i], \tag{4}$$

where m_k^i is the number of measurements obtained at sensor i at time k and $\mathbf{z}_{k,m}^i = [r_i^{k,m} \ \dot{r}_i^{k,m}]^T$. If target s is detected, the measurement $\mathbf{z}_k^{s,i}$ in (3) will be present in $\mathbf{Z}_k^i$ in (4). We define the probability that target s is detected at sensor i as $P_k^{s,i}$. We also define $\mathbf{Z}_k = [\mathbf{Z}_k^A \ \mathbf{Z}_k^B]$ as the full measurement at time k.

We assume that the number of false alarms at sensor i follows a Poisson distribution with average ρV_k^i, where ρ is the density of the clutter, and V_k^i is the validation gate volume [6]. The validation gate volume for target s at sensor i is $V_k^{s,i}$ and $V_k^i = \bigcup_{s=1}^S V_k^{s,i}$. The probability that m false alarms are obtained is

$$\mu(m) = \frac{\exp(-\rho V_k^i)(\rho V_k^i)^m}{m!}. \tag{5}$$

We also assume that the clutter is uniformly distributed in the volume V_k^i. The probability of detection at time k is modeled according to the relation

$$P_k^{s,i} = P_f^{\frac{1}{1+\eta_k^{s,i}}},$$

where P_f is the desired false alarm probability and $\eta_k^{s,i}$ is the SNR at sensor i corresponding to target s.

3. WAVEFORM STRUCTURE

In this section, we present the structure of the linear and nonlinear chirp waveforms used in this paper. We also describe the relationship between the transmitted waveform and the resulting measurement noise.

3.1. Waveform structure

At each sampling instant, each sensor transmits a generalized FM (GFM) pulse with complex envelope [4]

$$\tilde{s}(t) = a(t)\exp\left(j2\pi b\xi(t/t_r)\right), \qquad |t| < T/2 + t_f, \tag{6}$$

where b is a scalar FM rate parameter, $t_f \ll T/2$ is a rise/fall time for the trapezoidal envelope $a(t)$, and $t_r > 0$ is a reference time point. The phase function $\xi(t/t_r)$ is varied to yield a number of different time frequency signatures. The waveforms considered in this paper are the linear FM (LFM), power FM (PFM), hyperbolic FM (HFM)

Waveform	Phase Function $\xi(t)$	Frequency sweep
LFM	$t/\gamma + (t+\lambda/2)^2/2$	$b(\frac{1}{\gamma}+\lambda)$
PFM	$t/\gamma + (t+\lambda/2)^\kappa/\kappa$	$b(\frac{1}{\gamma}+\lambda)$
HFM	$\ln(t+\gamma+\lambda/2)$	$b\frac{\lambda}{\gamma(\gamma+\lambda)}$
EFM	$\exp(-(t+\lambda/2)/\gamma)$	$b\frac{1}{\gamma}(\mathrm{e}^{-\frac{\lambda}{\gamma}}-1)$

Table 1. FM waveforms used in the configuration scenarios.

and the exponential FM (EFM) chirps. The phase function and frequency sweep of each of these chirps are shown in Table 1 with the reference time[1] $t_r = 1$ and duration $\lambda = T + 2t_f$. In Table 1, the parameter γ helps to specify the instantaneous frequencies at the start and end of the pulse, given a duration λ and frequency sweep Δ_f. The waveform transmitted at time k by sensor i is thus parameterized by $\boldsymbol{\theta}_k^i = [\xi_k^i(t)\ \lambda_k^i\ b_k^i]^T$.

We choose the time-varying amplitude in (6) to have a trapezoidal structure as

$$a(t) = \begin{cases} \frac{\alpha}{t_f}(t - \frac{T}{2} - t_f), & -T/2 - t_f \le t < -T/2 \\ \alpha, & -T/2 \le t < T/2 \\ \frac{\alpha}{t_f}(\frac{T}{2} + t_f - t), & T/2 \le t < T/2 + t_f, \end{cases} \tag{7}$$

where α is an amplitude chosen so that $\tilde{s}(t)$ in (6) has unit energy. The choice of the trapezoidal envelope is discussed in [4].

3.2. Measurement noise covariance

Assuming a narrowband signal model [7], the signal reflected by target s undergoes a Doppler shift $\nu_k^{s,i}$ and is received at sensor i after a delay $\tau_k^{s,i}$. A matched filter in the receiver correlates the received waveform with delayed and frequency-shifted versions of the transmitted waveform. The magnitude of the correlation function in the absence of noise is given by the ambiguity function. The CRLB on the estimation of delay and Doppler can be obtained by inverting its Hessian, evaluated at the true target delay and Doppler [7]. The ambiguity function depends directly on the transmitted waveform, and we denote the Fisher Information matrix as $I(\boldsymbol{\theta}_k^i)$. Since $r_k^{s,i} = c\tau_k^{s,i}/2$ and $\dot{r}_k^{s,i} = c\nu_k^{s,i}/(2f_c)$, where c is the velocity of propagation and f_c is the carrier frequency, the CRLB for the estimation of range and range-rate of target s is given by

$$N^s(\boldsymbol{\theta}_k^i) = \frac{1}{\eta_k^{s,i}} \Gamma I(\boldsymbol{\theta}_k^i)^{-1} \Gamma^T,$$

where $\Gamma = \mathrm{diag}[c/2,\ c/(2f_c)]$.

[1] For the remainder of the paper, we assume that $t_r = 1$.

If the SNR is assumed to be high, the sidelobes of the ambiguity function can be neglected and the estimator can be assumed to achieve the CRLB [1]. We make this assumption and set the covariance of the measurement noise process $\mathbf{v}_k^{s,i}$ to $N^s(\boldsymbol{\theta}_k^i)$. We further assume that the measurement noise at each sensor for each target is independent.

4. TARGET TRACKING

The target tracker recursively estimates the probability distribution $p(\mathbf{X}_k|\mathbf{Z}_{1:k}, \boldsymbol{\theta}_{1:k})$ of the target state given the sequence of observations $\mathbf{Z}_{1:k}$ and waveform vectors $\boldsymbol{\theta}_{1:k}$ up to time k, where $\boldsymbol{\theta}_k = [\boldsymbol{\theta}_k^{A^T}\ \boldsymbol{\theta}_k^{B^T}]^T$ is a combined waveform parameter vector for both sensors at time k. Due to the nonlinearity in the observations model (3), we use a particle filter as the tracker [8]. This filter propagates a set of N_s particles and corresponding weights, $\{\mathbf{X}_k^j\ w_k^j\}, j = 1, \ldots, N_s$, in accordance with the kinematics model and the likelihood function. At each sampling instant, the particles are drawn from the kinematic prior $p(\mathbf{X}_k|\mathbf{X}_{k-1})$ and the weights are updated according to the likelihood as

$$w_k^j \propto w_{k-1}^j\ p(\mathbf{Z}_k|\mathbf{X}_k^j, \boldsymbol{\theta}_k). \tag{8}$$

Since the measurements obtained by each sensor are assumed to be independent, the likelihood function is

$$p(\mathbf{Z}_k|\mathbf{X}_k, \boldsymbol{\theta}_k) = \prod_{i=A,B} p(\mathbf{Z}_k^i|\mathbf{X}_k, \boldsymbol{\theta}_k^i). \tag{9}$$

When the targets are well separated in the observation space, the likelihood function factorizes into S components, one for each target, so that

$$p(\mathbf{Z}_k^i|\mathbf{X}_k, \boldsymbol{\theta}_k^i) = \prod_{s=1}^{S} p(\mathbf{Z}_k^{s,i}|\mathbf{x}_k^s, \boldsymbol{\theta}_k^i), \tag{10}$$

where $\mathbf{Z}_k^{s,i} \subset \mathbf{Z}_k^i$ is a set consisting of the observations in the validation gate of target s. Such a scenario corresponds to the case where the validation gates for each of the targets do not intersect. In this situation, the joint tracking of the targets reduces to tracking each target independently [9]. Assuming that each target produces at most one measurement, the likelihood functions in (10) are given by [10]

$$\begin{aligned} p(\mathbf{Z}_k^{s,i}|\mathbf{x}_k^s, \boldsymbol{\theta}_k^i) \quad &= \quad (1 - P_k^{s,i})\mu(n_s)(V_k^{s,i})^{-n_s} \\ &+ P_k^{s,i}(V_k^{s,i})^{-(n_s-1)}\mu(n_s-1)\frac{1}{n_s}\sum_{m=1}^{n_s} p_m^{s,i}, \end{aligned}$$

where n_s is the number of observations in the validation gate for target s and $p_m^{s,i} = p(\mathbf{z}_{k,m}^{s,i}|\mathbf{x}_k^s, \boldsymbol{\theta}_k^i)$ is the probability that the mth measurement in $\mathbf{Z}_k^{s,i}$ (or equivalently, the

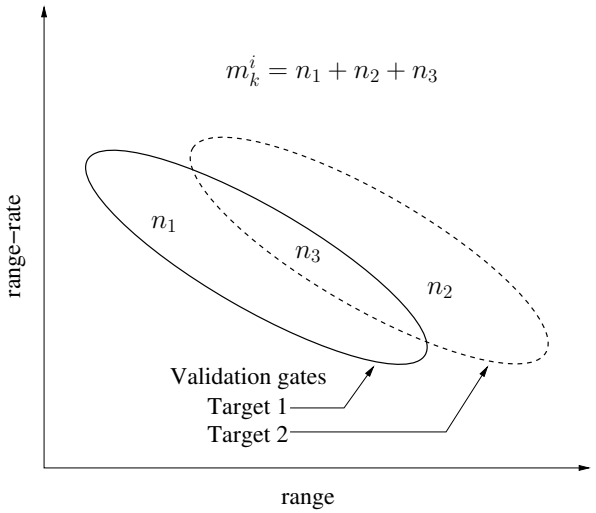

Fig. 1. Overlapping validation gates in observation space for 2 targets.

validation gate region for target s) was originated from the target s.

Figure 1 shows a scenario where the validation gates overlap for $S = 2$ targets. Here, n_1 and n_2 are the number of measurements that are validated exclusively for target 1 and target 2, respectively, while n_3 is the number of measurements validated for both targets. In this case, the factorization in (10) does not hold, and the tracker must estimate the states of each target jointly. We then have

$$p(\mathbf{Z}_k^i|\mathbf{X}_k, \boldsymbol{\theta}_k^i) = \sum_{r=1}^{R} p(\mathbf{Z}_k^i|\Omega_r, \mathbf{X}_k, \boldsymbol{\theta}_k^i) p(\Omega_r),$$

where Ω_r is the measurement-to-target association [6]. By exhaustively enumerating all possible associations when both targets, either target, or no targets are detected, it can be shown that

$$\begin{aligned} p(\mathbf{Z}_k^i|\mathbf{X}_k, \boldsymbol{\theta}_k^i) \quad &\propto \quad (1 - P_{d_k}^{1,i})(1 - P_{d_k}^{2,i}) \\ &+ \frac{m_k^i \rho^{-1} P_k^{1,i}(1 - P_k^{2,i})}{n_1 + n_3} \sum_{m=1}^{n_1+n_3} p_m^{1,i} \\ &+ \frac{m_k^i \rho^{-1} P_k^{2,i}(1 - P_k^{1,i})}{n_2 + n_3} \sum_{m=1}^{n_2+n_3} p_m^{2,i} \\ &+ \frac{m_k^i (m_k^i - 1) \rho^{-2} P_k^{1,i} P_k^{2,i}}{n_1 n_2 + n_2 n_3 + n_1 n_3} \sum_{l=1}^{n_1+n_3} \sum_{m=1}^{n_2+n_3} p_l^{1,i} p_m^{2,i}. \quad (11) \end{aligned}$$

Note that each target produces at most one measurement and the last summation in (11) must exclude all combinations that violate this fact. Although this was only shown for $S = 2$ targets, it can be extended to an arbitrary number of targets as in [6].

5. WAVEFORM SELECTION

The algorithm for waveform selection seeks the waveform for each sensor that minimizes the sum of the predicted MSE for all targets at the next time step. We define a cost function

$$J(\boldsymbol{\theta}_k) = E_{\mathbf{X}_k, \mathbf{Z}_k|\mathbf{Z}_{1:k-1}} \left((\mathbf{X}_k - \hat{\mathbf{X}}_k)^{\mathrm{T}} \boldsymbol{\Lambda} (\mathbf{X}_k - \hat{\mathbf{X}}_k) \right) \quad (12)$$

where $E(\cdot)$ denotes the an expectation over predicted states and observations, $\boldsymbol{\Lambda}$ is a weighting matrix that ensures that the units of the cost function are consistent, and $\hat{\mathbf{X}}_k$ is the estimate of $\mathbf{X}_k$ given the sequence of observations $\mathbf{Z}_{1:k}$. The minimization of $J(\boldsymbol{\theta}_k)$ in (12) is carried out by performing a progressively finer rectangular grid search over the space of allowable waveforms and determining the configuration that results in the lowest predicted cost [4]. The prediction of the MSE that would result if a particular waveform configuration was used is complicated by the nonlinear observations model, which implies that $J(\boldsymbol{\theta}_k)$ in (12) cannot be computed in closed form. We use an approach based on the unscented transform [11] to approximate it. The waveform selection procedure is described in more detail in [12]

5.1. Approximation of predicted MSE

The approximation of the predicted MSE using the unscented transform for a single target in clutter was presented in [4]. We now extend the algorithm to S targets. Let $P_{k-1|k-1}^s$ represent the covariance of the state estimate of target s at time $k-1$. We first obtain the predicted covariance at time k using the target dynamics model in (1) as

$$P_{k|k-1}^s = F P_{k-1|k-1}^s F^T + Q.$$

In order to obtain $P_{k|k}(\boldsymbol{\theta}_k)$, the estimate of the updated covariance that would result if a waveform parameterized by $\boldsymbol{\theta}_k$ was used at time k, we update each of the 4x4 block matrices $P_{k|k-1}^s$ sequentially for each sensor.

Sigma points $\boldsymbol{\mathcal{X}}_n^s, n = 1, \ldots, N$ are first computed from the probability density function whose mean and covariance are given by the predicted position of target s and $P_{k|k-1}^s$, respectively [11]. The sigma points are transformed to yield $\boldsymbol{\mathcal{Z}}_n^{s,i} = h^i(\boldsymbol{\mathcal{X}}_n^s)$. The covariance matrix $P_{zz}^{s,i}$ of $\boldsymbol{\mathcal{Z}}_n^{s,i}$, and the cross-covariance $P_{xz}^{s,i}$ between $\boldsymbol{\mathcal{X}}_n^s$ and $\boldsymbol{\mathcal{Z}}_n^{s,i}$ are computed. The updated covariance is computed as

$$P_{k|k}^{s,i}(\boldsymbol{\theta}_k^i) \quad = \quad P_{k|k-1}^s - q_{2_k}^{s,i} P_{k|k}^c \quad (13)$$

$$P_{k|k}^c \quad = \quad P_{xz}^{s,i} (P_{zz}^{s,i} + (N^s(\boldsymbol{\theta}_k^i))^{-1} P_{xz}^{s,i^T} \quad (14)$$

where $q_{2_k}^{s,i}$ is an information reduction factor [13]. The updates in (13) and (14) are performed for Sensor A to yield

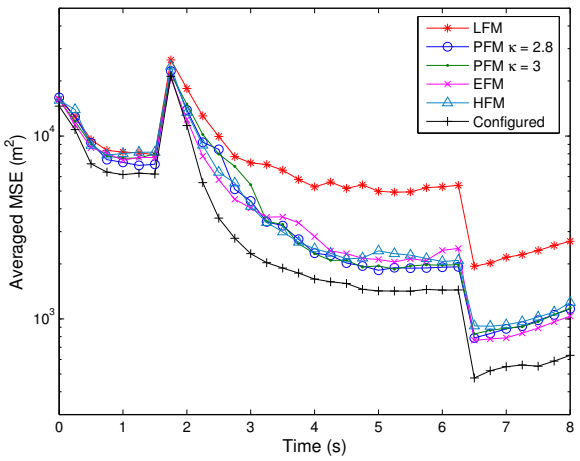

Fig. 2. Averaged MSE using waveforms with fixed and agile phase functions.

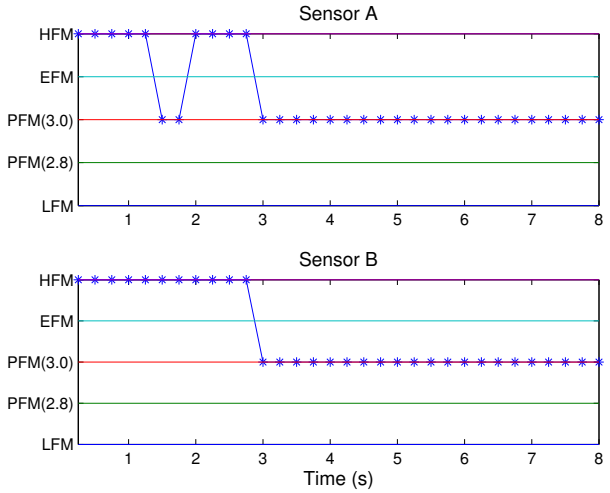

Fig. 3. Typical waveform selection during the tracking sequence.

$P^{s,A}_{k|k}(\boldsymbol{\theta}^A_k)$. The update for Sensor B follows the same procedure but with $P^s_{k|k-1}$ in (13) replaced by $P^{s,A}_{k|k}(\boldsymbol{\theta}^A_k)$ to yield $P^s_{k|k}(\boldsymbol{\theta}_k) = P^{s,B}_{k|k}(\boldsymbol{\theta}^B_k)$. Note that the covariance matrices in (14) must be re-evaluated for the second update. Once each of the $P^s_{k|k}(\boldsymbol{\theta}_k)$ has been evaluated, we form $P_{k|k}(\boldsymbol{\theta}_k) = \text{diag}[P^1_{k|k}(\boldsymbol{\theta}_k), \ldots, P^S_{k|k}(\boldsymbol{\theta}_k)]$ and obtain $J(\boldsymbol{\theta}_k) \approx \text{trace}(\Lambda P_{k|k}(\boldsymbol{\theta}_k))$.

6. SIMULATIONS

In order to demonstrate the application of the waveform selection algorithm to tracking multiple targets in clutter, we choose $S = 2$ in our simulations. In our simulation study, Sensor A and Sensor B are located at (3,000 -16,000) m and (3,000, 20,400) m respectively and track two targets as they move in a 2-dimensional space. The target trajectories are constructed with $\mathbf{x}^1_0 = [2000 \ -1000 \ -100 \ 800]^T$ and $\mathbf{x}^2_0 = [1000 \ -1000 \ 100 \ 800]^T$. In (2), $q = 1$ and the sampling interval is $\delta t = 0.25$ s. The clutter density is $\rho = 0.0001$ false alarms per unit validation gate volume while the probability of false alarm is $P_f = 0.01$. The SNR is modeled by $\eta^{s,i}_k = (50,000/r^{s,i}_k)^4$. The weighting matrix in (12) is the 8x8 identity matrix with appropriate units so that the MSE has units of m^2. Initially only target 1 is present in the observation space and target 2 is assumed to be detected at $k = 8$. Each target is tracked for 25 time steps (a total of 6.25 s). The initial position given to the tracker for target s is drawn from a normal distribution with mean $\mathbf{x}^s_0$ and variance $P_0 = \text{diag}(4{,}000, 4{,}000\ 100, 100)$. All results are averaged over 500 Monte Carlo runs, conditioned on convergence of the tracker. We define convergence to imply that the target-originated measurements for each target fall outside their validation gates at either sensor no more than five times during the entire tracking sequence.

Figure 2 shows the averaged MSE obtained using the waveform selection and configuration algorithm. The abrupt increase in the MSE at $k = 8$ (2 s) is due to the fact that the second target appears at this instant. Similarly, the drop in MSE at $k = 26$ (6.5 s) is due to the fact that the first target disappears at this time. For comparison, we also show the averaged MSE obtained when the waveform duration and FM rate may be configured dynamically but the phase function is fixed. We observe that, with phase function agility, the tracking performance improves. In particular, the performance is significantly better than that achieved by the LFM chirp, which is a common choice in radar applications.

A typical waveform selection during the tracking sequence is presented in Figure 3. Note that the waveforms selected include only the HFM and the PFM chirp with $\kappa = 3$, which corresponds to a parabolic instantaneous frequency. Interestingly, the LFM chirp is never selected. Also, the HFM chirp is chosen towards the initial stages while the PFM chirp is chosen towards the latter stages. This behavior is due to the fact that, at the start of the tracking, the uncertainty in position and velocity are both large and the range and range-rate have to be estimated independently; thus waveforms with minimal range-Doppler coupling should be expected to be chosen. It has been demonstrated that the HFM chirp has this feature, and is favored by bats and dolphins [14]. When the uncertainty in the target state estimate is reduced, it is possible to obtain a reduction in estimation errors by exploiting the range-Doppler coupling. The parabolic chirp has been shown to provide a lower variance on range errors conditioned on range-rate than the other chirps while still minimizing the validation gate volume [15].

Therefore the algorithm selects this waveform during the later stages of the tracking sequence. Note that this behavior is repeated when the second target appears at time $k = 8$. At this time, the uncertainty in the state estimate again increases and the algorithm chooses the HFM chirp to independently estimate the range and range-rate of target 2.

7. CONCLUSION

In this paper, we presented an algorithm to dynamically select the transmitted waveforms for two waveform-agile sensors that track multiple targets in clutter. The waveform selection is made so as to minimize the MSE which is predicted using the CRLB on the measurement error variance and the unscented transform to linearize the observations model. Using a simulation study, we demonstrated that the waveform selection improves tracking performance. We found, in particular, that the algorithm is responsive to the large changes in the tracking MSE that occur when targets appear or disappear. Since the waveform selection is driven by the tracker, the choice of waveforms reflects the uncertainty in the state estimate and adapts dynamically to the changing scenario. It is interesting to note that the behavior of our algorithm is similar to that of bats that dynamically adapt their transmitted waveforms during the search, approach, and capture of their prey [16].

8. REFERENCES

[1] D. J. Kershaw and R. J. Evans, "Optimal waveform selection for tracking systems," *IEEE Trans. Inform. Theory*, vol. 40, pp. 1536–1550, Sept. 1994.

[2] S. M. Hong, R. J. Evans, and H. S. Shin, "Optimization of waveform and detection threshold for range and range-rate tracking in clutter," *IEEE Trans. Aerosp. Electron. Syst.*, vol. 41, no. 1, pp. 17–33, Jan. 2005.

[3] S. D. Howard, S. Suvorova, and W. Moran, "Waveform libraries for radar tracking applications," *International Conference on Waveform Diversity and Design*, Nov. 2004.

[4] S. P. Sira, A. Papandreou-Suppappola, and D. Morrell, "Characterization of waveform performance in clutter for dynamically configured sensor systems," *International Waveform Diversity and Design Conference*, Jan. 2006, Hawaii, USA.

[5] D. J. Kershaw and R. J. Evans, "Waveform selective probabilistic data association," *IEEE Trans. Aerosp. Electron. Syst.*, vol. 33, pp. 1180–1188, Oct. 1997.

[6] Y. Bar-Shalom and T. E. Fortmann, *Tracking and Data Association*. Boston: Academic Press, 1988.

[7] H. L. Van Trees, *Detection Estimation and Modulation Theory, Part III*. New York: Wiley, 1971.

[8] M. S. Arulampalam, S. Maskell, N. Gordon, and T. Clapp, "A tutorial on particle filters for online nonlinear/non-Gaussian Bayesian tracking," *IEEE Trans. Signal Processing*, vol. 50, pp. 174–188, February 2002.

[9] C. Kreucher, K. Kastella, and Alfred O. Hero, III, "Multitarget tracking using the joint multitarget probability density," *IEEE Trans. Aerosp. Electron. Syst.*, vol. 41, no. 4, pp. 1396 – 1414, Oct. 2005.

[10] R. Niu, P. Willett, and Y. Bar-Shalom, "Matrix CRLB scaling due to measurements of uncertain origin," *IEEE Trans. Signal Processing*, vol. 49, no. 7, pp. 1325–1335, Jul. 2001.

[11] S. Julier and J. Uhlmann, "A new extension of the Kalman filter to nonlinear systems," *International Symposium on Aerospace/Defense Sensing, Simulation and Controls*, 1997.

[12] S. P. Sira, A. Papandreou-Suppappola, and D. Morrell, "Time-varying waveform selection and configuration for agile sensors in tracking applications," *IEEE International Conference on Acoustics, Speech, and Signal Processing*, vol. 5, pp. 881 – 884, Mar. 2005.

[13] T. Fortmann, Y. Bar-Shalom, M. Scheffe, and S. Gelfand, "Detection thresholds for tracking in clutter - A connection between estimation and signal processing," *IEEE Trans. Automat. Contr.*, vol. 30, pp. 221–229, Mar. 1985.

[14] R. A. Altes and E. L. Titlebaum, "Bat signals as optimally Doppler tolerant waveforms," *Journal of the Acoustical Society of America*, vol. 48, pp. 1014–1020, oct 1970.

[15] S. P. Sira, A. Papandreou-Suppappola, and D. Morrell, "Dynamic configuration of time-varying waveforms for agile sensing and tracking in clutter," *IEEE Trans. Signal Processing*, Submitted.

[16] J. A. Simmons and R. Stein, "Acoustic imaging in bat sonar: Echolocation signals and the evolution of echolocation," *Journal of Comparative Psychology*, vol. 135, no. 1, pp. 61–84, Mar. 1980.